Journal of Applied Polymer Science

Influence of polymer morphology on the adsorption behaviors of molecularly imprinted polymer-methacrylic acid functionalized β-cyclodextrin

Saliza Asman,[1,2] Sharifah Mohamad,[1] Norazilawati Muhamad Sarih[1]

[1]Department of Chemistry, Faculty of Science, University of Malaya, Lembah Pantai 50603, Kuala Lumpur, Malaysia

[2]Department of Science and Mathematics, Faculty of Science, Technology and Human Development, University of Tun Hussein Onn Malaysia 86400, Parit Raja Johor, Malaysia

Correspondence to: S. Mohamad (E-mail: sharifahm@um.edu.my)

ABSTRACT: The influence of molecularly imprinted polymer-methacrylic acid functionalized β-cyclodextrin (MIP(MAA-β-CD)) morphology on the adsorption behavior studies towards benzylparaben (BzP) was explored. The effects of time, concentration, and temperature towards BzP uptake were extensively evaluated. The adsorption performance of MIP(MAA-β-CD) was compared with that on the molecularly imprinted polymer-methacrylic acid (MIP(MAA)) synthesized without β-CD. The MIP(MAA-β-CD) was synthesized to obtain a spherical and spongy-porous texture with a broad pore size distribution. The MIP(MAA-β-CD) showed fast kinetic and the intra-particle diffusion model demonstrated a three step (surface and pore) adsorption process. The Koble-Corrigan isotherm was the most suitable model for data fitting, which indicated that MIP(MAA-β-CD) had homogeneous and heterogeneous surfaces. This finding clearly demonstrated that the large uptake and strong affinity of MIP(MAA-β-CD) did not only probably result from the monomer-template interactions, but also due to the morphological MIP(MAA-β-CD) structure. In contrary to MIP(MAA-β-CD), MIP(MAA) synthesized with uniform morphology and narrow pore size distribution had lower adsorption capacities and its kinetic data fitted the pseudo-second order diffusion model, indicating a two-step (surface only) adsorption process. The MIP(MAA) adsorption process followed the Langmuir isotherm model referred to solely homogeneous uptake. The calculated thermodynamic parameters showed that the BzP uptake was exothermic, spontaneous, and physisorption process onto MIPs, which supported the results of kinetics and isotherm adsorption data. This study clearly revealed that the presence of β-CD improved the morphology of synthesized MIP, and automatically enhanced the adsorption behavior of MIP. © 2015 Wiley Periodicals, Inc. J. Appl. Polym. Sci. **2015**, *132*, 42720.

KEYWORDS: adsorption; functionalization of polymers; kinetics; morphology

Received 25 May 2015; accepted 7 July 2015

DOI: 10.1002/app.42720

INTRODUCTION

Molecularly imprinted polymers (MIPs) have become a promising technology to make receptor-like polymers based on the molecular recognition theory.[1] It was developed rapidly in recent years due to ease in preparation, thermal and chemical stability, and high selectivity. The technique of MIPs is based on three main steps; (i) self-assembly of template and monomer molecules, (ii) polymerization of template-monomer complex with cross-linking agent, and (iii) template removal to create binding cavity that is specific to the imprint molecule.[2] MIPs can be used in many different fields such as separation,[3] catalyst,[4] and sensor.[5] Over the past decade, significant inroads have been made towards elucidating the nature of the molecular level mechanisms governing the recognition characteristics of MIPs material.[6] However, the performance of MIPs is not only dictated by the monomer-template interaction on a molecular level, but also by the physical make-up of the polymer on a macromolecular level. MIPs are generally insoluble materials, which subsequent use depends on their morphology in terms of the particle shape and size, and the porous texture of the materials.[7] Hence, the morphology of MIPs can affect their subsequent molecular recognitions and adsorption behaviors for selected analyte, thus directly suitable to their mode of application.

To date, the advances in molecular imprinting technology (MIT) have led to the development of novel synthetically engineered MIPs material that is incorporated with cyclodextrins (CDs) within an imprinted polymeric framework, which fortunately improved the performance of MIPs.[8–10] CDs are glucose-based molecules, produced from the enzymatic degradation of

starch by bacteria. They are cyclic oligosaccharides, consisting of six (α), seven (β), and eight (γ) glucopyranose units, which are joined together by α-(1,4)-glycosidic linkage bonds, forming a torus-shaped ring structure.[11] The exterior sides of them are hydrophilic for the outward hydroxyl groups, while the interior cavities are hydrophobic, so they can behave as hosts for various molecules. The most significant feature of CDs is the ability to form inclusion compounds with various organic molecules through host-guest interactions in aqueous media.[12] Besides, the incorporation of CDs within the framework structure of adsorbent materials represents a novel modular design approach with significant potential for controlling tuning of the textural mesoporosity of such macromolecular level.[13] Furthermore, CDs were used as potential pore templates to form microporous and nanoporous materials because of their well-defined structure, versatility, and the ability to form inclusion and interfacial complexes.[12,14] Among the CDs types, β-cyclodextrin (β-CD) is the most recently used in various synthetic adsorbent materials as it is conveniently accessible and comes in low price.[15] The preparation of MIPs based on β-CD as monomer has previously been reported to be successful.[16–18] The orientation of β-CD molecule residues in the MIPs are placed complementary to the template and the assembled β-CD molecules can work as a whole to recognize the template precisely.[19] On the other hand, the modification of a typical monomer with β-CD is another innovative strategy. By linking several functional groups of typical monomer to β-CD, a number of possible bonds can be created between the template and the monomers, while the recognition ability could be improved as it increases the binding capacity of MIPs.

In our previous work,[20] a molecularly imprinted polymer (MIP) was prepared based on modified monomer-β-CD material for selective recognition of benzylparaben (BzP) analyte, which represented as molecularly imprinted polymer-methacrylic acid functionalized β-cyclodextrin (MIP(MAA-β-CD)). The modification of methacrylic acid (MAA) with β-CD was initially a process to obtain a newly functionalized monomer named methacrylic acid functionalized β-cyclodextrin (MAA-β-CD). A significant study on the monomer-template interaction was derived from NMR and 2D NOESY analysis of potential pre-polymerization mixtures. The result proved that the high recognition capacity of MIP(MAA-β-CD) was exhibited due to the triple mechanism interactions (inclusion complex, hydrogen bonding, and π–π interaction) created.

While our understanding of the impact of molecular level factor related to the pre-polymerization stage; by exploiting of β-CD in molecular imprinting polymerization has developed. The relationship between the polymer morphologies and corresponding polymer adsorption behaviors has been relatively unexplored. As promising, the β-CD provides an innovative design strategy for the development of "smart" or "functional" porous adsorbent materials due to their unique physicochemical properties.[13] Therefore, we believed that the morphology property of MIPs, based on modified monomer-β-CD provided useful physicochemical parameters for achieving the optimal polymer design for sorption-based applications.

Herein, we report the use of MIP(MAA-β-CD) for the sorption of BzP, in relation to the influence of MIP(MAA-β-CD) morphology towards the adsorption behavior studies. To the best for our knowledge, study on the relationships between polymer morphology with adsorption behaviors of MIP based on modified monomer-β-CD have yet to be reported. Hence, batch kinetic, equilibrium adsorption, and thermodynamic experiments were conducted. The results of this sorption studies would contribute to better understanding of the sorption behavior of MIP with commensurate polymer morphology towards BzP uptake, thus its potential can be utilized in aqueous media. A typical molecularly imprinted polymer-methacrylic acid (MIP(MAA)) without β-CD was synthesized as reference.

EXPERIMENTAL

Materials and Reagents

β-cyclodextrin (β-CD) was purchased from Acros (Geel, Belgium). Methacrylic acid (MAA), toluene-2,4-diisocyanate (TDI), trimethylolpropane trimethacrylate (TRIM), benzyol peroxide (BPO), dimethylacetamide (DMAC), 2,2-phenyl-2-propyl benzodithioate (PPDT), dibutyltin dilaurate (DBTDL), benzylparaben (BzP), methanol, acetic acid, and toluene were purchased from Sigma-Aldrich (Buches SG, Switzerland). Other solvents were analytical reagent grade and were used as received without further purification. Distilled water was used throughout the experiments.

Synthesis of Methacrylic Acid Functionalized β-Cyclodextrin (MAA-β-CD)

Methacrylic acid functionalized β-cyclodextrin (MAA-β-CD) monomer was prepared based on our previous work.[20]

Synthesis of Molecularly Imprinted Polymers (MIPs)

The MIPs were synthesized based on our previous work.[20] The MIP(MAA-β-CD) was synthesized via reversible addition-fragmentation chain transfer (RAFT) polymerization process due to its versatile process[21–23] in bulk polymerization method. The BzP template (0.14 mmoL) was dissolved in 10 mL of DMAC solvent in a flask, containing MAA-β-CD monomer (0.56 mmoL), TRIM cross-linker (2.80 mmoL), BPO initiator (0.15 g), and PPDT as RAFT agent (1.24 mmoL). The solution was sealed and purged with nitrogen gas for at least 10 min. Then, the mixture was allowed to polymerize in a water bath at 70°C for overnight. The obtained bulk MIP(MAA-β-CD) was crushed, ground, and wet-sieved. The extraction process was carried out with a mixture of methanol/acetic acid (v/v, 9/1) to leach out the BzP template from MIP(MAA-β-CD) until the BzP template in the eluate could no longer be detected at a wavelength of 258 nm by the UV–Vis spectrophotometer. The particles were then extensively washed with methanol to remove any residual acetic acid and were dried under vacuum at 80°C. The MIP(MAA) was synthesized and treated with the same method using 0.56 mmoL of MAA monomer and 10 mL of toluene as a solvent, with the absence of β-CD.

Characterization of MIPs

The surface morphology of the MIPs was determined using Quanta FEG 450 Field Emission Scanning Electron Microscope (FESEM) from FEI (Hillsboro, OR). The surface area and pore size distribution of the MIPs were measured by nitrogen adsorption–desorption analysis at 77 K using Quantachrome

Autosorb Automated Gas Sorption system (Quantachrome, Boynton Beach, FL). Prior to nitrogen sorption measurements, the MIPs were previously degassed at 393 K for 24 h to remove adsorbed gases and moisture. The specific surface area of MIPs was calculated from Brunauer-Emmett-Teller (BET). Meanwhile, the Barrett-Joyner-Halenda (BJH) method was applied to calculate the average pore size of MIPs from the adsorption–desorption branches of the isotherms, whereas the Dubinin-Radushkevich (DR) plots were applied to calculate the pore volume of MIPs. The concentration of BzP in the aqueous solution was analyzed using a Shimadzu Ultraviolet–Visible spectroscopy (UV–Vis) recording spectrophotometer (Shimadzu, Tokyo, Japan), equipped with 1 cm quartz cells at a maximum wavelength of the BzP ($\lambda_{max} = 258$ nm).

Batch Adsorption Studies of MIPs

Adsorption Kinetics. Kinetic studies were applied to study the effect of contact time and to calculate the kinetic parameter. Hence, in order to determine the effect of time on BzP uptake, the adsorption process was conducted for the time interval of (5, 10, 15, 30, 60, 90, 120, 150, and 180) minutes at 298 K. The initial concentration of BzP was fixed at 10 mg L^{-1} in 20 mL of BzP solution, and was shaken mechanically with 0.05 g dosage of MIPs in a water bath shaker. Each test was done thrice as parallel experiments and the experimental data were the mean of their results. The BzP uptake at time (t) defined as binding capacity, Q_t (mg/g), was calculated using eq. (1).

$$Q_t = \frac{[(C_0 - C_t) \times v]}{w} \quad (1)$$

where Q_t is the binding capacity of MIPs (mg/g), C_0 and C_t are the initial and any time of BzP solutions (mg/L), respectively, v (L) is the volume of BzP solution, and w (g) is the mass of MIPs particles used.

Adsorptions Isotherms. In order to study the equilibrium isotherm of the adsorption, various initial concentrations of BzP were studied (10, 50, 100, 150, 200, and 250 mg/L) under three varying temperatures (298, 318, and 338 K) using the optimized time. The solution of BzP was shaken mechanically in a water bath shaker with 0.05 g dosage of MIPs in 20 mL of BzP solution. Each test was done thrice as parallel experiments and the experimental data were the mean of their results. The BzP uptake at equilibrium defined as binding capacity, Q_e (mg/g) was calculated using eq. (2).

$$Q_e = \frac{[(C_0 - C_e) \times v]}{w} \quad (2)$$

where Q_e is the binding capacity of MIPs (mg/g), C_0 and C_e are the initial and equilibrium concentrations of BzP solutions (mg/L), respectively, v (L) is the volume of BzP solution, and w (g) is the mass of MIPs particles used.

Adsorption Kinetic Models. The kinetics of BzP adsorption onto the MIPs were analyzed using pseudo-first order, pseudo-second order, Elovich model, external particle diffusion, intra-particle diffusion, and Boyd model. The conformity between the experimental data and the model predicted values was expressed by the correlation coefficients (R^2). A relatively high R^2 value (close or equal to 1) was used to indicate the best fit to the kinetic model.

Pseudo-first order equation. The pseudo-first order equation is generally presented as follows:

$$\log (q_e - q_t) = \log q_e - \frac{k_1(t)}{2.303} \quad (3)$$

where q_e (mg g^{-1}) is the amount of BzP adsorbed at equilibrium; q_t (mg g^{-1}) is the amount of BzP adsorbed at time, t and k_1 is the pseudo-first order rate constant (min^{-1}). The values of log (q_e–q_t) are plotted against t, while k_1 and q_e values are calculated from the slope and the intercept of the plot, respectively.

Pseudo-second order equation. The pseudo-second order equation is defined as:

$$\frac{t}{q_t} = \frac{1}{h} - \frac{t}{q_e} \quad (4)$$

where $h = k_2 q_e^2$ (mg g^{-1} min^{-1}) is the initial sorption rate and k_2 (g mg^{-1} min^{-1}) is the rate constant of pseudo-second order kinetic. The values of k_2 and q_e can be calculated from the slope and the intercept of the graph t/qt against t. The half adsorption time, $t_{1/2}$ (min) is another parameter and it is defined as the time required for the adsorption to take up half as much compound as its equilibrium values. It is an effective measurement of sorption rate.[24] The equation is presented as:

$$t_{\frac{1}{2}} = \frac{1}{k_2 q_e} \quad (5)$$

Elovich model. The Elovich model is represented as:

$$q_t = 1 \ln (\alpha\beta) + \frac{1}{\beta} \ln t \quad (6)$$

where α (mg g^{-1} min^{-1}) is the initial sorption rate and β (g mg^{-1}) is related to the extended surface coverage and activation energy for chemisorptions. The values of α and β can be obtained by a plot of q_t against ln t. This model is applicable when the plot of q_t against ln t represents a straight line.[25]

External diffusion model. The external diffusion model can be written as equation:

$$ln \frac{C_t}{C_0} = -k_{ext}(t) \quad (7)$$

where C_0 (mg L^{-1}) and C_t (mg L^{-1}) are the concentrations of the BzP solute in the initial solution and in the liquid phase, respectively, at time, t. The k_{ext} (min^{-1}) is the diffusion rate parameter for film diffusion model and can be evaluated from the slope of the linear plot of $ln\ C_t/C_0$ against t.

Intra-particle diffusion model. Weber and Morris described a functional relationship of intra-particle diffusion[26] as the eq. (8):

$$q_t = k_i \left(t^{\frac{1}{2}} \right) + IP \quad (8)$$

where k_i (mg g^{-1} $min^{1/2}$) is the particle diffusion rate constant and IP (mg g^{-1}) is the effect of the boundary layer thickness constant. The value of k_i and IP can be determined from the slope and the intercept of the linear plot of q_t against $t_{1/2}$, respectively.

Boyd model. The Boyd model is expressed to determine either the adsorption process is the intra-particle diffusion or the external particle diffusion.[25] The rate-limiting step in the adsorption process could be interpreted as intra-particle diffusion if the plot of B_t against t is a straight line passing through the origin. The Boyd model can be written in eqs. (9) and (10):

$$If\ \ 0.86 < F < 1;\ \ B_t = -0.49770 - \ln(1-F); \tag{9}$$

$$If\ \ 0 < F < 0.85; B_t = \left(2\pi - \frac{\pi^2}{3}\right) - 2\pi\left[1 - \left(\frac{\pi F}{3}\right)\right]^{0.5} \tag{10}$$

where B_t is the Boyd parameter and F is the fraction of solute adsorbed at any time, t as calculated using $F = q_t/q_e$.

Validation of the kinetic model. The suitability of the model to describe the adsorption kinetics was further justified by predicting the normalized standard deviation value, Δq (%) and relative error (%), which are defined as eqs. (11) and (12), respectively.

$$\Delta q\% = \sqrt{\frac{\left[\left(q_{exp} - q_{cal}\right) q_{exp}\ \right]^2}{\mathrm{N}-1}} \tag{11}$$

$$Relative\ \ error\ \ (\%) = \frac{|q_e cal - q_e exp|}{\mathrm{q}_e exp} \times 100 \tag{12}$$

where N is the number of data points, $q_{e\ exp}$ (mg g^{-1}) and $q_{e\ cal}$ (mg g^{-1}) are the experimental and calculated adsorption capacity, respectively. Generally, the model fits better if the value of Δq is lower.

Adsorption Isotherm Models. In this study, linearized two-parameter equations (Langmuir, Freundlich, Temkin, and Dubinin-Radushkevich isotherm models) and linearized three-parameter equation (Koble-Corrigan isotherm model) were examined for their ability to model the equilibrium sorption data. The parameters resulted from the models provide significant information on the sorption mechanism and the surface property and affinity of the adsorbent.

Langmuir isotherm model. The Langmuir isotherm model is described by the following eq. (13) as depicted in the following:

$$\frac{c_e}{q_e} = \frac{c_e}{q_m} + \frac{1}{bq_m} \tag{13}$$

where C_e (mg L^{-1}) is the equilibrium concentration of BzP adsorbate; q_m (mg g^{-1}) is the maximum sorption capacity; and b (L mg^{-1}) is the Langmuir constant related to the energy of sorption. q_m and b are the Langmuir constants that are related to the monolayer adsorption capacity and affinity of adsorbent towards adsorbate, respectively. The values of q_e and b can be calculated from the slope and intercept, respectively, by the equation of the linear plot of C_e/q_e against C_e. Furthermore, in order to predict the adsorption efficiency of the process, the dimensionless equilibrium parameter was determined by the following equation:

$$R_L = \frac{1}{1 + bC_0} \tag{14}$$

where C_0 (mg L^{-1}) is the initial concentration of adsorbate. The R_L value indicates the shape of the isotherm: (1) $R_L > 1$, unfavorable adsorption, (2) $R_L = 1$, linear adsorption, (3) $0 < R_L < 1$, favorable adsorption, and (4) $R_L = 0$, irreversible adsorption.

Freundlich isotherm model. The Freundlich isotherm model is described by the eq. (15) as portrayed in the following:

$$\log q_e = \log c_e \left(\frac{1}{n}\right) + \log k_f \tag{15}$$

where n is the Freundlich constant for intensity and K_f (mg g^{-1}) is the Freundlich constant for sorption capacity. The values of K_f and n can be calculated from the slope and the intercept of the plot between log q_e against log C_e.

Temkin isotherm model. The Temkin isotherm equation is shown in eq. (16):

$$q_e = \beta\ ln\ K_T + \beta\ lnC_e \tag{16}$$

where $\beta = RT/\ b_T$; R (kJ mol^{-1} K^{-1}) is the universal gas constant; T (Kelvin) is the temperature; K_T (L mg^{-1}) is the Temkin constant related to the equilibrium binding energy; and b_T (J mol^{-1}) is the Temkin constant related to the heat of adsorption. K_T and b_T can be determined from the intercept and the slope from q_e against ln C_e plot.

Dubinin-Radushkevich isotherm model. The Dubinin-Radushkevich isotherm equation was determined by the following equation:

$$lnq_e = lnq_m - \beta\varepsilon^2 \tag{17}$$

where β (mol^2 kJ^{-2}) is the adsorption energy constant obtained from the slope of the plot ln q_e against ε^2, where ε is the Polanyi potential. The ε value and the mean free energy, E (kJ/mol) could be calculated from eqs. (18) and (19).

$$\varepsilon = RT\ln\left[1 + \frac{1}{c_e}\right] \tag{18}$$

$$E = \left(2\beta^{-0.5}\right) \tag{19}$$

Koble-Corrigan isotherm model. The Koble-Corrigan equation is represented in eq. (20) as following below:

$$\frac{1}{q_e} = \left(\frac{1}{A_k C e^P}\right) + \frac{B_k}{A_k} \tag{20}$$

where A_k, B_k, and P are the Koble-Corrigan model constants.

Adsorption Thermodynamics. In any adsorbate-adsorbent adsorption system, the values of thermodynamic parameters such as enthalpy change ($\Delta H°$), entropy change ($\Delta S°$), and free energy change ($\Delta G°$) are important indicators to determine the spontaneity of a process. The thermodynamic parameters can be estimated using equilibrium constant that changes with temperature. Besides, the standard free energy change ($\Delta G°$) of the sorption reaction can be calculated from the following below:

$$\Delta G^0 = -RT\ln K_d \tag{21}$$

where R is the ideal gas constant = 8.314 $Jmol^{-1}$ K^{-1} and K_d is the distribution coefficient or equilibrium constant (g L^{-1}). Meanwhile, the K_d value can be computed with eq. (22) as below:

$$K_d = \frac{q_e}{C_e} \tag{22}$$

The values of enthalpy ($\Delta H°$) and entropy changes ($\Delta S°$) can be identified from the Van't Hoff plot (ln K_d vs. $1/T$) by

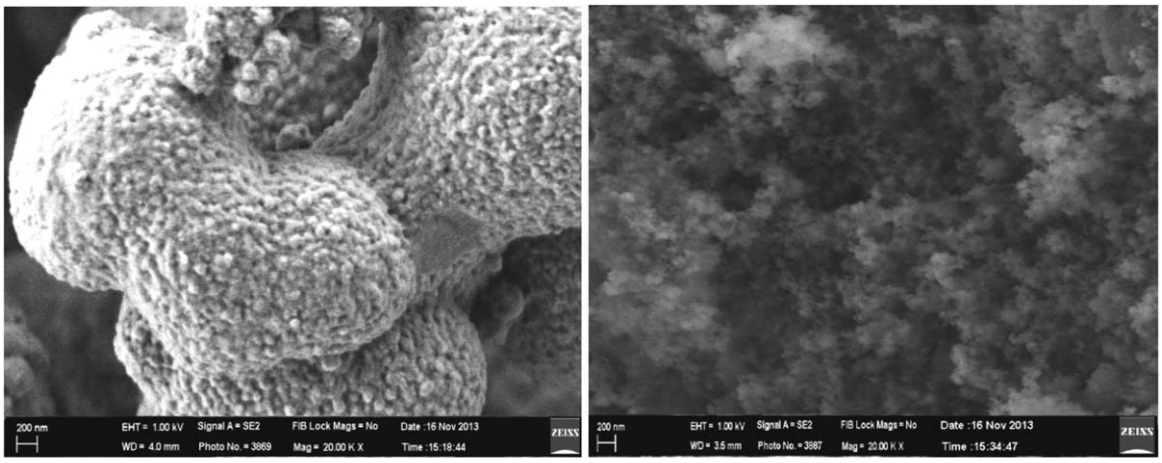

Figure 1. FESEM images of (a) MIP(MAA-β-CD) and (b) MIP(MAA).

calculation from the slope and intercept, respectively, using the eq. (23) below:

$$\ln K_d = \frac{-\Delta G^0}{RT} = \frac{-\Delta H^0}{RT} + \frac{\Delta S^0}{R} \quad (23)$$

RESULTS AND DISCUSSION

Characterization of MIPs

The microscopic morphological structures of MIPs were investigated using Field Emission Scanning Electron Microscope (FESEM) under 20,000× magnification, as depicted in Figure 1. Significant differences between MIP(MAA-β-CD) and MIP (MAA) were noticed in the morphological images. The surface of MIP(MAA-β-CD) formed a spherical and spongy-porous structure, while the MIP(MAA) exhibited a uniform structure. These different morphologies confirmed the successful attachments of β-CD in the MIP(MAA-β-CD) polymer matrix. Besides, the β-CD, which was fully accommodated inside the entire MIP(MAA-β-CD) polymer matrix, strongly affected the morphology design. The globular structures were obtained in MIP(MAA-β-CD) particles, which might be caused by the adsorbed water due to the β-CD hydrophilic characteristic that interrupted the polymer network.[27] Hence, the globular structure remained after water was removed in dry state.

Samples of MIPs were characterized using BET and the physicochemical properties of each are summarized in Table I. MIP (MAA-β-CD) exhibited low BET surface area (11.31 m^2/g) compared to MIP(MAA), confirming that the addition of β-CD into the imprinted polymer matrix has isolated inside the internal surface of the polymer matrix, thus decreased the surface area value of MIP(MAA-β-CD) in the dry state. The large BET surface area of MIP(MAA) (426.9 m^2/g) described the typical value for the surface area of the MIP, which was basically in the range of 100–400 m^2/g.[28] The total pore volume of MIP(MAA-β-CD) was lower than those of MIP(MAA), proving the hydrogel nature of MIP(MAA-β-CD).[20] Thus, the particle size of MIP(MAA-β-CD) could theoretically increase after swelling.[24] The calculated average pore sizes at around 2–50 nm diameters confirmed the mesopores particles of MIPs.

Table I. Physicochemical Properties of MIPs

Polymers	BET surface area, S (m^2/g)	Total pore volume, V_p (cm^3/g)	Average pore size, d_p (nm)
MIP(MAA-β-CD)	11.31	4.20×10^{-4}	8.67
MIP(MAA)	426.9	0.7	7.14

The N_2 adsorption/desorption isotherms of MIPs (Figure 2) exhibited a resolved Type-IV isotherm with hysteresis loops, indicating the existence of many mesopores in the polymers. The Type H3 adsorption hysteresis loop of MIPs suggested that the polymers obtained aggregates of plates, which gave rise to the slit-shape mesoporous.[29] Different desorption hysteresis loops pattern showed that the MIP(MAA-β-CD) [Figure 2(a)] exhibited Type H1, which demonstrated an agglomerated or compacted spheroidal particle.[30] On the other hand, the Type H4 desorption hysteresis loop indicated that the MIP(MAA) [Figure 2(b)] obtained a narrow slit-like pores particle.[31] In addition, a different surface area size of polymers could be determined from the increasing volume of adsorbed N_2 ($cm^3 g^{-1}$). A higher volume of adsorbed N_2 indicated a large surface area of MIP(MAA) (426.9 m^2/g), compared to those with low surface area MIP(MAA-β-CD) (11.31 m^2/g). Nevertheless, the amount of N_2 adsorbed rose sharply at high pressure ($P/P_0 > 0.9$) for MIP(MAA-β-CD), which suggested the presence of an appreciably high textural inter-particle porosity in low surface area material.[12,13] Meanwhile, the rapid increase of N_2 adsorbed at high pressure ($0.4 < P/P_0 < 0.9$) for MIP(MAA) revealed a delayed condensation, which indicated a small pore size homogenous polymer.[24] A BJH pore size distribution plot [Figure 2(c)] produced from the desorption isotherms demonstrated the presence of differences in pore size distributions between the MIP(MAA-β-CD) and MIP(MAA). Despite having slightly similar average pore sizes to MIP(MAA), MIP(MAA-β-CD) differed in that it had a broad pore size distribution as large as mesopores particles (46.68 nm). Meanwhile, two pore

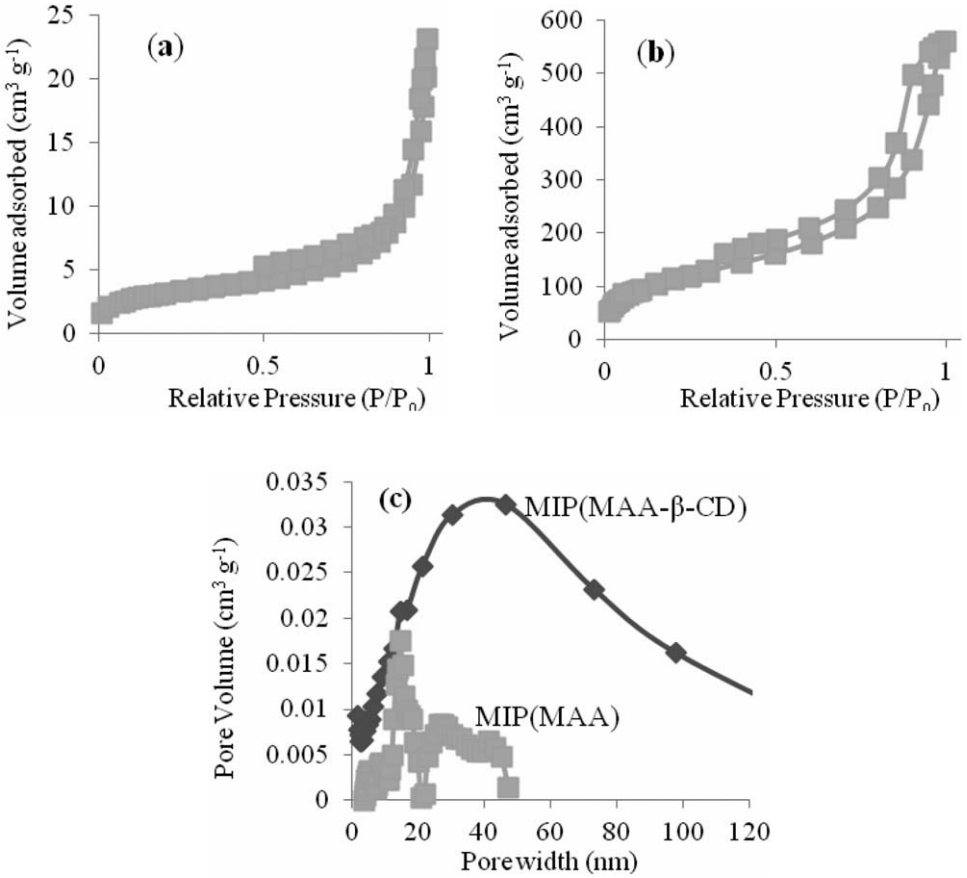

Figure 2. Nitrogen adsorption/desorption profiles of (a) MIP(MAA-β-CD) and (b) MIP(MAA); (c) BJH pore size distribution plots of MIPs.

size distributions were found for MIP(MAA), whereby the first was a narrow distribution at 14.73 nm and the second was a low broad distribution at 26.46 nm, indicating a well-defined narrow pore size mesopores range.

Adsorption Kinetics

Figure 3 shows the kinetic effect of BzP adsorbed onto MIPs. The plots of MIPs illustrated similar shapes and equilibrium trends. The sorption process was rapid in the initial stage at 5 min, and gradually increased until it slowed down near the equilibrium at 15 min, and remained constant after that. Theoretically, the fast uptake of BzP in the beginning might be attributed to the rapid attachment of BzP molecules on the surface of MIPs, since a large number of vacant sites of MIPs were available, and the BzP concentration was high. After a certain period, the remaining vacant sites were difficult to occupy due to repulsive force between BzP molecules on the MIPs surface phase. A few active sites were available, and the solution concentration decreased. Hence, BzP uptake happened very slowly until it reached equilibrium.

In addition, adsorption kinetics explains the rate of adsorbate uptake on MIPs. Pseudo-first order (a first-order rate equation to describe the kinetic process of liquid–solid adsorption), pseudo-second order (the main assumptions were that the adsorption might be second-order, and the rate limiting step might be related to chemical adsorption involving valent forces through sharing or the exchange of electrons between the adsorbent and the metal ions),[32] and Elovich kinetic (to prove that the sorption was based on the chemisorption process)[33] models were applied to gain insight pertaining to the kinetics of adsorption process of BzP. The kinetic parameters calculated from the slopes and the intercepts of the plots from these models are listed in Table II. It was discovered that the pseudo-second order model fits the kinetic adsorption of BzP better

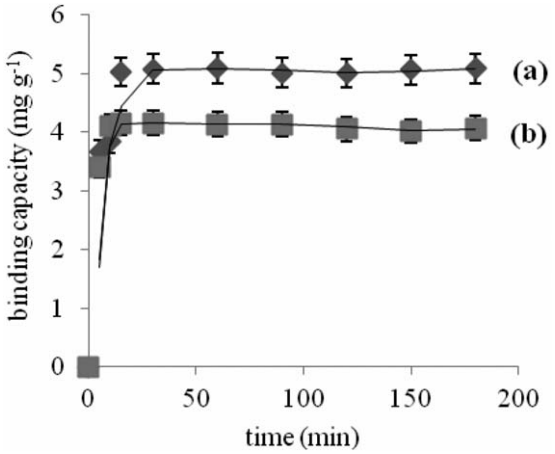

Figure 3. Effect of kinetic on the adsorption of BzP onto (a) MIP(MAA-β-CD) and (b) MIP(MAA), (Adsorption conditions: MIPs dose = 50 mg, initial concentration = 10 mg/L, solution volume = 20 mL, T = 298 K, time = 1 h).

Table II. Kinetic Parameters for the Adsorption of BzP onto MIPs

Kinetic model	Parameter	MIP(MAA-β-CD)	MIP(MAA)
Pseudo-first order kinetic model	q_e, *exp* (mg/g)	5.0941	4.1559
	q_e, *cal* (mg/g)	1.5007	0.7191
	k_1 (min^{-1})	0.0283	0.0122
	h_1	0.0425	8.773E-03
	Δq_t	5.921	1.981
	Relative error (%)	70.54	82.70
	R^2	0.9894	0.9072
Pseudo-second order kinetic model	q_e, *cal* (mg/g)	5.0994	4.1684
	k_2 (g/mg min^{-1})	0.1983	0.1835
	h_2 (mg/g min)	5.1573	3.1888
	$t_{1/2}$ (min)	0.9889	1.3074
	Δq_t	5.779	1.707
	Relative error (%)	0.10	0.30
	R^2	0.9998	0.9997
Elovich model	q_e, *cal* (mg/g)	5.2789	4.1594
	β (g mg^{-1})	2.8417	10.6045
	α (mg g^{-1} min^{-1})	6.40E+03	7.50E+15
	Δq_t	1.57	0.231
	Relative error (%)	3.63	0.08
	R^2	0.6262	0.2583

than other models for MIPs based on R^2 values. Besides, the theoretical $(q_e)_{cal}$ values were found to be in accordance with the experimental uptake $(qe)_{exp}$ values. The lower values of Δq_t and relative errors (%) of the pseudo-second order kinetic model resulted in a better model fit.[33] Compared to MIP (MAA), the high initial sorption rate values (h) and low values of time required for the adsorption at ($t_{1/2}$) proved that the MIP(MAA-β-CD) was a better adsorbent. This might occur due to the presence of β-CD moiety in the internal surface of MIP (MAA-β-CD), which resulted in a broad pore diameter and lower pore volume of polymer matrix, proving that the super pores enhanced the mass transport for BzP analyte. Moreover, the hydrogel nature of MIP(MAA-β-CD) completed with its high swelling capacity in water and with many cavities, making its network expandable to allow rapid diffusion process for the adsorbed BzP analyte. In other words, the broad pore structures reduced the diffusion distance transport, resulting in faster mass transfer performance,[34] proving the adsorption kinetic was mainly controlled by pore structure through the MIP(MAA-β-CD) adsorbent. Nonetheless, the adsorption system disagreed with the pseudo-first order model, since the theoretical $(q_e)_{cal}$ values did not give any reasonable value with regard to the experimental uptake $(q_e)_{exp}$, even though the R^2 values were acceptable. The R^2 values of Elovich model were too low, rendering its inapplicability and unacceptable.

Further kinetic information was obtained by application of the external diffusion, intra-particle diffusion, and Boyd models (Figure 4) to study the diffusion mechanism of the adsorption process and to predict the rate-controlling step. Figure 4(a) represents the external diffusion model that was employed to determine the linear relation plots of MIPs during the initial stages. Both plots displayed small intercept values, which suggested that the external film diffusion was the rate-controlling step of the initial fast adsorption of BzP onto MIPs. The intra-particle diffusion model for the adsorption mechanism of BzP onto MIPs can be identified in Figure 4(b). Theoretically, the adsorption kinetic was controlled by three consecutive mass transport steps associated with the adsorption of solute from the solution by an adsorbent.[35] These included (1) film diffusion, where the straight line that passed through the origin indicated the adsorption of the adsorbate was instantaneous and extremely fast uptake of the most readily available sites on the adsorbent external surface; (2) intra-particle or pore diffusion, as well as the migration of adsorbate from the fluid phase to the adsorbent internal surface; and (3) sorption into interior sites, where the adsorption of the particles began to slow down due to the extremely low adsorbate concentration. Since the third step had been very rapid, the film and the pore diffusion transports were the two major steps that strongly controlled the rate of adsorption. These three steps were observed for the adsorption of BzP onto MIP(MAA-β-CD). These results provided the first experimental evidence that MIP(MAA-β-CD) with large pore size distributions supported the coordination of BzP species onto the polymer surface and inside the pores. Meanwhile, two steps were observed for the adsorption of BzP onto MIP(MAA). This

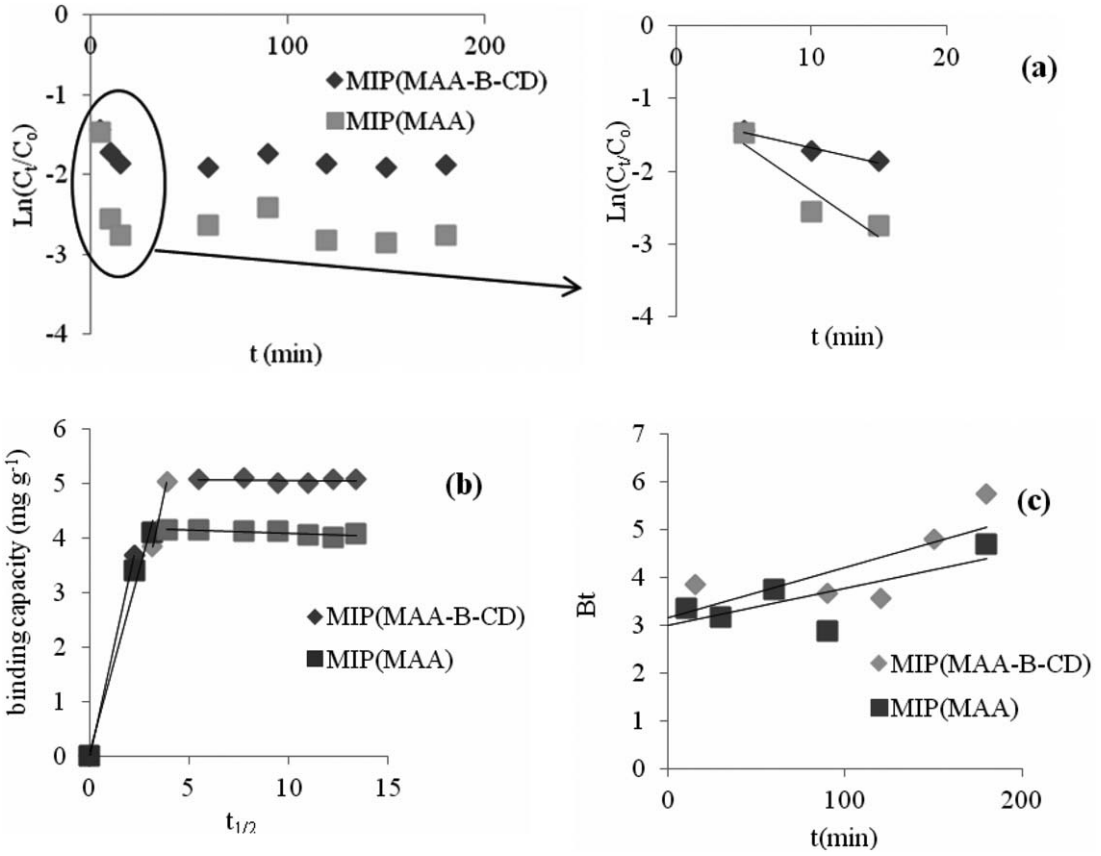

Figure 4. (a) External particle diffusion, (b) internal particle diffusion, and (c) Boyd model for adsorption of BzP onto MIP(MAA-β-CD) and MIP(MAA).

Table III. Rate Constant of External Diffusion and Intra-particle Diffusion Models for Adsorption of BzP onto MIPs

Adsorbents	External diffusion model	Intra-particle diffusion model					
	k_{ext}	k_{p1}	k_{p2}	k_{p3}	IP_1	IP_2	IP_3
MIP(MAA-β-CD)	0.129	0.473	0.048	0.001	2.105	3.765	5.045
MIP(MAA)	0.042	0.140	0.021	-	2.697	4.222	-

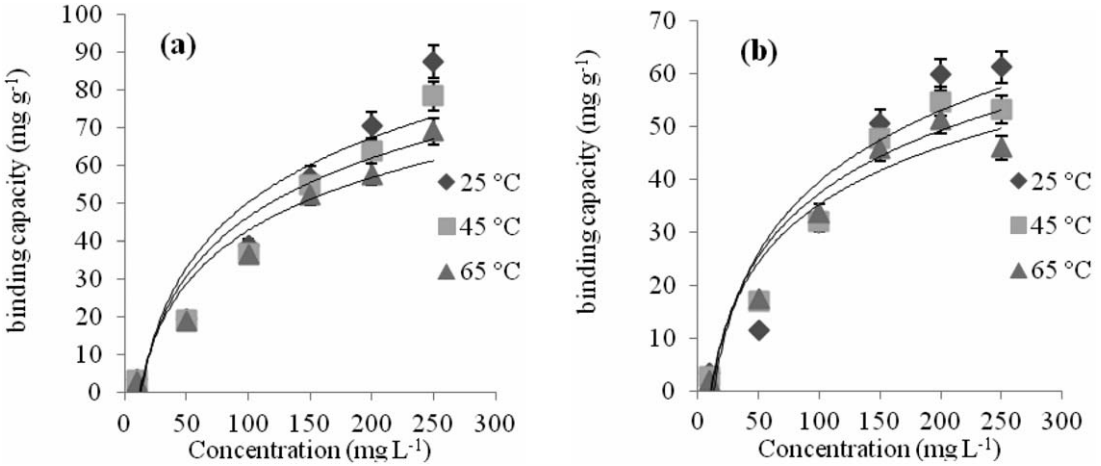

Figure 5. Sorption isotherm for adsorption of BzP onto (a) MIP(MAA-β-CD) and (b) MIP(MAA).

Table IV. Isotherm Constants and Correlation Coefficients of Various Isotherms Models for Adsorption of BzP onto MIPs

		MIP(MAA-β-CD)			MIP(MAA)		
Adsorption model	Parameter	25°C	45°C	65°C	25°C	45°C	65°C
Langmuir	q_e *exp* (mg/g)	87.62	78.49	72.74	61.21	54.76	51.18
	R^2	0.9622	0.9946	0.983	0.9012	0.8202	0.9401
	b (L/mg)	0.0874	0.0798	0.0527	0.0298	0.0311	0.0322
	q_m *cal* (mg/g)	106.38	91.74	85.47	87.72	71.43	59.52
	R_L	$0.04 < R_L < 0.56$	$0.04 < R_L < 0.56$	$0.07 < R_L < 0.66$	$0.1 < R_L < 0.78$	$0.1 < R_L < 0.77$	$0.07 < R_L < 0.65$
	Δq_e	0.16	0.07	0.07	0.25	0.35	0.34
Freundlich	R^2	0.9054	0.9715	0.9794	0.8332	0.8286	0.7078
	K_F (mg^{1-m} L^m g^{-1})	15.02	13.13	9.84	2.11	1.22	0.85
	n	2.11	2.24	2.17	1.25	1.09	1.04
	1/n	0.4731	0.4461	0.4618	0.7983	0.914	0.9619
	Δq_e	0.18	0.09	0.11	0.15	0.04	0.02
Temkin	R^2	0.9523	0.9966	0.9815	0.9439	0.9089	0.8035
	K_T (L/g)	1.05	0.91	0.57	0.64	0.4	0.36
	B (J/mol)	21.72	18.9	18.12	15.74	15.87	14.61
	Δq_e	2.39	2.66	1.61	0.06	0.28	0.81
Dubinin-Radushkevich	R^2	0.9859	0.9902	0.9731	0.9595	0.8858	0.951
	q_D *cal* (mg/g)	74.41	65.78	56.32	50.48	40.3	42.83
	B	2.57	5.04	5.52	2.47	7.19	14.87
	E(kJ/mol)	1.25	0.89	0.85	1.35	0.75	0.52
	Δq_e	0.51	0.42	0.43	0.99	0.52	0.36
Koble-Corrigan	R^2	0.8982	0.9979	0.9937	0.3257	0.5703	0.5891
	p	1.0	1.2	1.1	0.92	1.01	1.02
	A_k	9.73	8.39	5.34	1.03	1.49	1.74
	B_k	0.091	0.099	0.069	0.002	0.012	0.021
	Δq_e	0.66	0.71	0.49	0.15	0.09	0.08

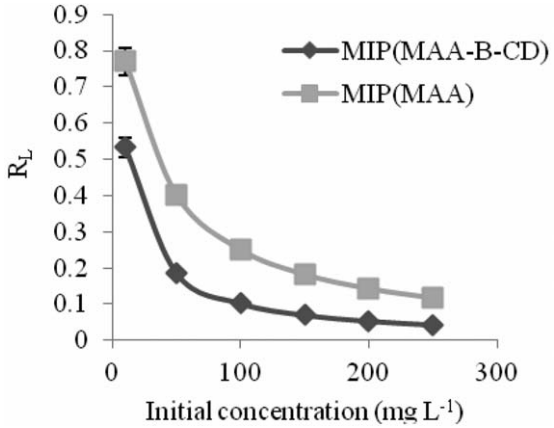

Figure 6. Values of R_L for adsorption of BzP onto MIPs at 25°C.

result suggested that pore diffusion was the rate-determining step for adsorbents with broad pore size distributions, but not for those that contained a narrow pore size distribution range.[32] Furthermore, the k_{pi} and IP_i values (Table III) denoted that BzP diffused faster through the external and the internal surfaces of MIP(MAA-β-CD) than MIP(MAA). It might be attributed to their different structures. The different structures of MIPs showed that the MIP(MAA-β-CD) best fit for BzP. The existence of different regions indicated that both external diffusion and intra-particle diffusion models occurred simultaneously. Therefore, Boyd kinetic model [Figure 4(c)] was used to determine the slowest step in the overall adsorption process. It can be seen that the plots did not pass through the origin, and the slightly scattered points were obtained, which means that the film diffusion was the rate-controlling step.[25]

Adsorption Isotherms

The adsorption isotherm study of MIPs was carried out with various concentrations and temperatures. The binding isotherm of BzP showed that the amount of BzP bound to the MIPs (Figure 5) at the equilibrium increased with concentration until it reached a saturation level. Nevertheless, the adsorption of BzP decreased as the temperature increased, and it was suspected that the adsorption system favored lower temperatures.

The adsorption isotherm study was performed to describe the distribution of adsorption molecules between the liquid (adsorbate) and the solid phases (adsorbent) when the adsorption process reached an equilibrium state. The linearized forms of Langmuir, Freundlich, Temkin, Dubinin-Radushkevich, and Koble-Corrigan models were applied to determine the fit of the equilibrium data. Table IV compiled the fitting results for modeling BzP adsorption. The calculated q_m values using the Langmuir model of MIPs had been higher than the q_e experimental values. However, it was still indicative of the fact that BzP uptake possessed higher affinity with MIP(MAA-β-CD) than MIP(MAA), due to the b (L mg^{-1}) values. The R^2 values (mostly above 0.9) revealed that the Langmuir isotherm model seemed to provide homogeneous system with better fitting for both MIPs. The R^2 of MIP(MAA-β-CD) exceeded the R^2 of MIP(MAA), confirming that the MIP(MAA-β-CD) was more homogeneous. Besides, the separation factor, R_L values (Table IV) were all in the range between 0 and 1, indicating that the adsorption processes had been favorable over the range of initial BzP concentrations being applied. Moreover, it was discovered that the degree of favorability (Figure 6) for MIP(MAA-β-CD) was superior to MIP(MAA). At high BzP concentrations, the decrease in R_L values indicated a less significant role in adsorption.

Apart from that, the Freundlich model indicated that the K_f values of MIP(MAA-β-CD) were large, proving that the MIP(MAA-β-CD) had greater adsorption capacity and possessed more heterogeneity binding sites. The n values above unity and $1/n$ values far less from 1 showed that the MIP(MAA-β-CD) was a favorable adsorbent with relatively strong bonds formation between the adsorbate and the adsorbent. In addition, the R^2 values indicated that the MIP(MAA-β-CD) system was heterogeneous. It could be possibly assumed that MIP(MAA-β-CD) participated in heterogeneous system. In contrary to MIP(MAA), the values of K_f were too low and the values of $n<2$ with $1/n \approx 1$ revealed that the adsorption system of MIP(MAA) was limited and unfavorable. These results suggested that the MIP(MAA) was inapplicable evaluated by Freundlich isotherm. Meanwhile, the Temkin model displayed that the MIP(MAA-β-CD) had more affinity and was strongly present in the monolayer uniform adsorption than MIP(-MAA) due to R^2 values. The constant K_T and B values, related to the heat of sorption on MIP(MAA-β-CD), were found to be higher than MIP(MAA), might be due to the varying interaction mechanism of the adsorption systems. In addition, the Dubinin-Radushkevich (D-R) model also proved that the adsorption of BzP had been more favorable towards MIP(MAA-β-CD) than MIP(MAA) because the q_D calculated values of MIP(MAA-β-CD) were higher than MIP(MAA). In addition, the D-R model was related to the free energy (E) of adsorption per adsorbate when transferred to the surface of the solid from infinity in the solution, allowing for predicting the type of adsorption.[25] Since the E values were all small (Table IV), a possible physisorption process between adsorbent and adsorbate could be proposed. As a conclusion, the adsorption equilibrium data (two-parameter isotherm model) of MIP(MAA-β-CD) fit the isotherm models in the order of: Langmuir > Temkin > Dubinin-Radushkevich > Freundlich.

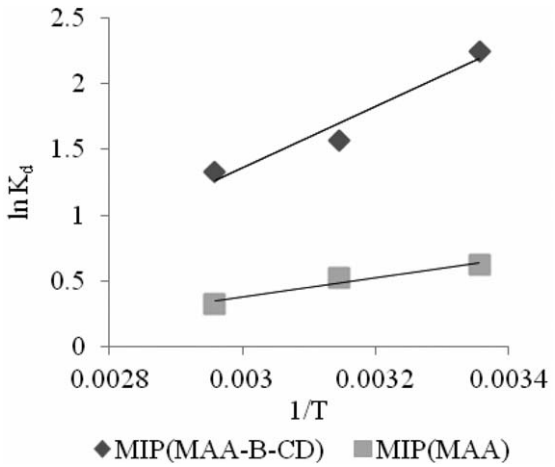

Figure 7. Van't Hoff plots for adsorption of BzP onto MIPs.

Table V. The Calculated Values of Thermodynamic Parameters for MIPs

Adsorbents	Temperature (°C)	Enthalpy $\Delta H°$ (kJ/mol)	Entropy $\Delta S°$ (J/Kmol)	Gibbs energy $\Delta G°$ (J/mol) × 10^3
MIP(MAA-β-CD)	25	−19.43	−47.00	−5.57
	45			−4.14
	65			−3.74
MIP(MAA)	25	−6.1	−15.2	−1.53
	45			−1.37
	65			−0.91

Besides, the Koble-Corrigan model (three-parameter isotherm model) showed better correlation with the experimental adsorption than the two-parameter isotherm model. The best fitting for Koble-Corrigan model (R^2 values) with the experimental equilibrium data confirmed the combination of heterogeneous and homogeneous uptakes for BzP through MIP(MAA-β-CD) (agreed with Langmuir and Freundlich isotherm models). This could possibly derive from the morphology structure of MIP(MAA-β-CD); the MIP(MAA-β-CD) had homogeneous and heterogeneous surfaces, with many cavities, proving the influence of β-CD on polymer matrix. Again, the β-CD had strongly improved the morphology surface of MIP(MAA-β-CD) and directly enhanced its adsorption behaviors. Comparing the coefficients of determination of the Freundlich and Langmuir models, we infer that homogeneous uptake was the main mechanism for the BzP adsorption process. The values of $p \approx 1$ revealed that the adsorption reaction stoichiometry would be 1 solute molecule per free adsorbent site.[36] These results suggested that BzP was mainly adsorbed onto MIP(MAA-β-CD) by 1 : 1 mechanism (monolayer sorption). Meanwhile, the Koble-Corrigan model did not fit to MIP(MAA) equilibrium data, revealing that the MIP(MAA) only participated in homogeneous uptake, referring to the results obtained from the Langmuir model.

Adsorption Thermodynamics

Figure 7 shows the Van't Hoff plot for the BzP uptake onto MIPs. The calculated values of the thermodynamic parameters are shown in Table V. The negative values of $\Delta H°$ for MIPs indicated the exothermic nature of the adsorption process. The $\Delta H°$, which ranged between 2.1 and 20.9 kJ mol^{-1}, confirmed that MIP (MAA-β-CD) (19.43 kJ mol^{-1}) and MIP(MAA) (6.1 kJ mol^{-1}) were in physisorption process. Additionally, the energy values, which were taken from the D-R isotherm model, had been consistent with these results. The higher magnitude values of $\Delta H°$, $\Delta S°$, and $\Delta G°$ for MIP(MAA-β-CD) compared to MIP(MAA) might be related to the difference in the mechanisms of the adsorption system. In addition, the negative values of $\Delta S°$ for MIPs indicated the decreased randomness of the interface of solid solution during sorption.[37] It revealed that the adsorption of BzP onto MIPs was driven mainly by enthalpy changes. Besides, the negative magnitude values of $\Delta G°$ suggested a spontaneous nature of the adsorption process. The absolute $\Delta G°$ values decreased as the temperature increased, indicating that the adsorption of BzP molecules became less favorable at higher temperatures.[38] This might be due to the increasing trend of desorbing BzP from the interface to the solution, or the distorted active sites on the adsorbent.[39] Furthermore, the larger absolute values of $\Delta G°$ for MIP(MAA-β-CD), as opposed to MIP(MAA) suggested stronger adsorptive affinity of BzP to MIP1, which was consistent with the n values from Freundlich isotherm. These findings support the results retrieved from adsorption kinetics and isotherms data.

CONCLUSIONS

The investigation on the influence of MIP(MAA-β-CD) morphology towards adsorption behavior studies of BzP uptake was carried out extensively. The results were compared with MIP(-MAA) produced without β-CD. The results showed that the spherical and spongy porous MIP(MAA-β-CD) with broad size pore distribution demonstrated faster kinetic rate compared to MIP(MAA). Moreover, the three-step intra-particle diffusion mechanism process was observed. The Koble-Corrigan model was shown to provide the best fitting for MIP(MAA-β-CD) equilibrium data. In contrary to MIP(MAA-β-CD), the uniform MIP(MAA) morphology with narrow pore size distribution provided slow kinetic rate, defined by the two-step intra-particle diffusion mechanism process. The Langmuir isotherm model was fitted well for MIP(MAA) equilibrium system. Hence, this study proved that the presence of β-CD improved the morphology of MIP(MAA-β-CD) and directly enhanced the adsorption behavior of BzP uptake. It clearly proved that the large uptake and the strong affinity of MIP(MAA-β-CD) did not only probably result from the monomer-template interactions, but a clear link between the influence of morphology and the subsequent adsorption behavior performance of MIPs was displayed.

ACKNOWLEDGMENTS

Financial support from the Postgraduate Research Fund (IPPP) grant (PV015-2011A) and the Research Grant (UMRG) program (RP006A-13SUS) under the University of Malaya, and scholarship support from the Malaysian Ministry of Education are gratefully acknowledged.

REFERENCES

1. Dong, X.; Wang, N.; Wang, S.; Zhang, X.; Fan, Z. *J. Chromatogr. A* **2004**, *1057*(1–2), 13.
2. Piacham, T.; Nantasenamat, C.; Suksrichavalit, T.; Puttipanyalears, C.; Pissawong, T.; Maneewas, S.; Isarankura-Na-Ayudhya, C.; Prachayasittikul, V. *Molecules* **2009**, *14*(8), 2985.

3. Cheong, W. J.; Yang, S. H.; Ali, F. *J. Sep. Sci.* **2013**, *36*(3), 609.
4. Sergeyeva, T. A.; Slinchenko, O. A.; Gorbach, L. A.; Matyushov, V. F.; Brovko, O. O.; Piletsky, S. A.; Sergeeva, L. M.; Elska, G. V. *Anal. Chim. Acta* **2010**, *659*(1–2), 274.
5. Hillberg, A. L.; Brain, K. R.; Allender, C. J. *Adv. Drug Deliv. Rev.* **2005**, *57*(12), 1875.
6. Rosengren, A.; Karlsson, B.; Nicholls, I. *Int. J. Mol. Sci.* **2013**, *14*(1), 1207.
7. Holland, N.; Frisby, J.; Owens, E.; Hughes, H.; Duggan, P.; McLoughlin, P. *Polymer* **2010**, *51*(7), 1578.
8. Piletsky, S. A.; Andersson, H. S.; Nicholls, I. A. *Macromolecules* **1999**, *32*(3), 633.
9. Matsui, T.; Osawa, T.; Shirasaka, K.; Katayama, M.; Hishiya, T.; Asanuma, H.; Komiyama, M. *J. Inclu. Phenom. Macrocyclic Chem.* **2006**, *56*(1–2), 39.
10. Guo, W.; Hu, W.; Pan, J.; Zhou, H.; Guan, W.; Wang, X.; Dai, J.; Xu, L. *Chem. Eng. J.* **2011**, *171*(2), 603.
11. Ozmen, E. Y.; Yilmaz, M. *J. Hazard. Mater.* **2007**, *148*(1–2), 303.
12. Asouhidou, D. D.; Triantafyllidis, K. S.; Lazaridis, N. K.; Matis, K. A. *Colloids Surf. A* **2009**, *346*(1–3), 83.
13. Wilson, L. D.; Mohamed, M. H.; Headley, J. V. *J. Colloid Interface Sci.* **2011**, *357*(1), 215.
14. Polarz, S.; Antonietti, M. *Chem. Commun.* **2002**, (*22*), 2593.
15. Chin, Y. P.; Mohamad, S.; Abas, M. R. B. *Int. J. Mol. Sci.* **2010**, *11*(9), 3459.
16. Hishiya, T.; Akiyama, T.; Asanuma, H.; Komiyama, M. *J. Inclu. Phenom. Macrocyclic Chem.* **2002**, *44*(1–4), 365.
17. Tsai, H.-A.; Syu, M.-J. *Biomaterials* **2005**, *26*(15), 2759.
18. Ma, Y.; Pan, G.; Zhang, Y.; Guo, X.; Zhang, H. *J. Mol. Recogn.* **2013**, *26*(5), 240.
19. Xu, Z.; Xu, L.; Kuang, D.; Zhang, F.; Wang, J. *Mater. Sci. Eng. C* **2008**, *28*(8), 1516.
20. Asman, S.; Mohamad, S.; Muhamad Sarih, N. *Int. J. Mol. Sci.* **2015**, *16*(2), 3656.
21. Moad, G.; Rizzardo, E.; Thang, S. H. *Aust. J. Chem.* **2005**, *58*(6), 379.
22. Cormack, P.; MehAMod, F. S. *Sains Malays.* **2013**, *42*(4), 529.
23. Li, Y.; Li, X.; Chu, J.; Dong, C.; Qi, J.; Yuan, Y. *Environ. Pollut.* **2010**, *158*(6), 2317.
24. Li, N.; Mei, Z.; Wei, X. *Chem. Eng. J.* **2012**, *192*, 138.
25. Castro López, M.; Cela Pérez, M. C.; Dopico García, M. S.; López Vilariño, J. M.; González Rodríguez, M. V.; Barral Losada, L. F. *Anal. Chim. Acta* **2012**, *721*, 68.
26. Ahmed, M. J.; Theydan, S. K. *Ecotoxicol. Environ. Saf.* **2012**, *84*, 39.
27. Kyzas, G. Z.; Lazaridis, N. K.; Bikiaris, D. N. *Carbohydr. Polym.* **2013**, *91*(1), 198.
28. Spivak, D. A. *Adv. Drug Deliv. Rev.* **2005**, *57*(12), 1779.
29. Ma, X.; Li, L.; Yang, L.; Su, C.; Wang, K.; Yuan, S.; Zhou, J. *J. Hazard. Mater.* **2012**, *209–210*, 467.
30. Toth, B.; Laszlo, K.; Horvai, G. *J. Chromatogr. A* **2005**, *1100*(1), 60.
31. Sing, K. S. *Pure Appl. Chem.* **1985**, *57*(4), 603.
32. Idris, S. A.; Alotaibi, K. M.; Peshkur, T. A.; Anderson, P.; Morris, M.; Gibson, L. T. *Microporous Mesoporous Mater.* **2013**, *165*, 99.
33. Raoov, M.; Mohamad, S.; Abas, M. R. *J. Hazard. Mater.* **2013**, *263*, Part 2, 501.
34. Du, K.-F.; Yan, M.; Wang, Q.-Y.; Song, H. *J. Chromatogr. A* **2010**, *1217*(8), 1298.
35. Bhatnagar, A.; Minocha, A. *J. Hazard. Mater.* **2009**, *168*(2), 1111.
36. Alahmadi, S.; Mohamad, S.; Maah, M. *Molecules* **2014**, *19*(4), 4524.
37. Aydın, Y. A.; Aksoy, N. D. *Chem. Eng. J.* **2009**, *151*(1), 188.
38. Wang, X.; Pan, J.; Guan, W.; Dai, J.; Zou, X.; Yan, Y.; Li, C.; Hu, W. *J. Chem. Eng. Data* **2011**, *56*(6), 2793.
39. Kilic, M.; Apaydin-Varol, E.; Pütün, A. E. *J. Hazard. Mater.* **2011**, *189*(1), 397.